IEEE Access
Multidisciplinary | Rapid Review | Open Access Journal

Received July 22, 2019, accepted August 4, 2019, date of publication August 9, 2019, date of current version August 22, 2019.

Digital Object Identifier 10.1109/ACCESS.2019.2934135

Design, Measurement and Analysis of Near-Field Focusing Reflective Metasurface for Dual-Polarization and Multi-Focus Wireless Power Transfer

PEI ZHANG, LONG LI, (Senior Member, IEEE), XUANMING ZHANG, HAIXIA LIU, (Member, IEEE), AND YAN SHI, (Senior Member, IEEE)

Key Laboratory of High Speed Circuit Design and EMC of Ministry of Education, School of Electronic Engineering, Collaborative Innovation Center of Information Sensing and Understanding, Xidian University, Xi'an 710071, China

Corresponding authors: Long Li (lilong@mail.xidian.edu.cn) and Haixia Liu (hxliu@xidian.edu.cn)

This work was supported by the Science and Technology Project of State Grid Corporation of China through the Research on Ten-meter level Microwave Radio wireless power Transmission Technology.

ABSTRACT A new design of dual-polarization and multi-focus near-field focusing (NFF) reflective metasurface for wireless power transfer (WPT) system is proposed in this paper. In terms of multi-beam phase synthesis of reflective metasurface, the dual-polarization metasurface with independent regulation characteristics is introduced to realize multi-focus and high-efficiency WPT. The single-feed single-focus and the single-feed dual-focus metasurface working at X-band (10 GHz) with 26 × 26 elements in two polarizations are designed, fabricated and measured by planar near-field scanning experiments. Furthermore, a compact antenna is designed and fabricated as the receiver to form a practical WPT system. The measurement results show that a NFF transfer system is 15 dB higher than a non-NFF transfer system. Through full-wave simulation and experiments of three cases, single focus, dual-focus, and single focus with dual-polarization can respectively realize the maximum focusing efficiency of 71.6%, 68.3% and 65.9%. The relative bandwidth with 50% power focusing efficiency of these three cases are all about 12%, which demonstrates the stability and feasibility of the NFF reflective metasurface for practical WPT applications.

INDEX TERMS Near-field focusing, reflective metasurface, wireless power transfer, multi-focus, dual-polarization.

I. INTRODUCTION

Since electric energy has become the main energy source in human society, it has always been a dream to realize wireless power transfer (WPT). According to the working mechanism, WPT systems [1] can be divided into magnetic induction [2], magnetic coupling resonance [2] and microwave transmission systems [3]. Among these, the former two have been on the road to commercialization, which can be respectively applied to small electronic devices within range of 10 cm and large-sized equipment such as vehicles [4]. However, for long-distance transfer of more than 1m, it can only be realized by means of microwave transmission. The propagation of microwaves in space is accompanied by large attenuation and loss, thus how to efficiently transfer microwave power becomes the core issue of long-distance WPT. In the far-field region, the traditional high-gain directional beam can solve the problem of long-distance and high-power, but the power distribution is divergent, and the aperture of the whole system is also large and costly.

Near-field focusing (NFF) [5], [6] is a property of Fresnel and near regions of antennas, theoretically speaking, which can converge electromagnetic waves from the transmitting source at a certain point in near-field region within the outer boundary of $2D^2/\lambda$. Since its introduction in the last century, NFF has been implemented through various antenna structures, such as, parabolic reflector [7], dielectric lens antennas [8], microstrip phased array [9]–[12], planar FZP(Fresnel zone plate) lens [13], [14] and so on. But the processing difficulty of parabolic reflector, the complexity of microstrip

The associate editor coordinating the review of this article and approving it for publication was Ildiko Peter.

array, and the low-efficiency of planar FZP(Fresnel zone plate) lens, all these problems hinder the development of NFF for WPT. In recent years, microstrip leaky-wave antenna [15], [16] is proposed to make a simpler alternative solution to phased-arrays. Therefore, the transmitter which can both take into account efficiency and cost remains to be further explored

On the other hand, WPT needs to meet the practical needs of more diversification and flexibility. How to better control the focused beam has attracted the attention of researchers. In 2013, [17] attempted control the amplitude excitation to reduce unwanted secondary lobes through Gaussian arrays, and based on the higher order Bessel beams methods, achieved multi-focused beams in the near-field by a 20 GHz circular antenna array. In 2016, [18] put forward a Ka-band NFF array with SIW(substrate integrated waveguide) technology, whose metallic circular holes are designed as both phase shifters and radiating elements. A side-lobe of less than -18 dB was obtained by properly arranging the dimensions of the metallic circular holes. In 2017, [20] proposed a reconfigurable holographic metasurface aperture to realize dynamic NFF. In 2018, [19] presented an 8×8 microstrip array which has a steerable focal distance from 78 to 249 mm achieved as frequency varies from 9.25 to 10.5 GHz.

Since this century, the research of metasurface [20], [21], [24]–[26] has opened a brand-new gate for the orderly regulation of electromagnetic waves. Through the periodic or aperiodic arrangement of sub-wavelength electromagnetic structures, the amplitude, phase and polarization properties can be effectively regulated. Among these, each element of the metasurface is phase-compensated according to its optical path difference compared with an in-phase point in space, that beam direction can be controlled, which makes the power focused in an aperture within the near-field region. A NFF reflective array for RFID(radio frequency identification devices) system at 2.4 GHz was proposed [22] to obtain a focus at the range of 2m. Some scholars have introduced the NFF metasurface for underwater ultrasonic [23] and mid-infrared waves [24]. In 2018, [25] proposed a new design of NFF metasurface for high-efficiency WPT with multi-focus characteristics, which lays a solid foundation for multi-point NFF for long-distance WPT.

In this paper, a dual-polarization NFF reflective metasurface is presented with cross-dipole structure to realize the independent control of polarization. Combined with multi-beam reflection method, it is better to meet the actual needs of WPT multi-focus power allocation and multi-source power synthesis. Two NFF reflective metasurfaces working at 10 GHz with the size of 390 mm$\times$390 mm are designed for single-feed single-focus and single-feed dual-focus in different polarizations, respectively. The near-field scanning measurement results show that this design achieves a good function of wireless power diversity. A 4×4 mushroom metasurface antenna is designed as the receiver to form a WPT system to verify the effectiveness of NFF. Finally, some characteristics of NFF are analyzed by full-wave simulation to further clarify the focusing performance for long-distance WPT.

II. DESIGN OF DUAL-POLARIZATION METASURFACE ELEMENT

In order to achieve dual-polarization independent regulation, and to take the fabrication cost into consideration, the metasurface element used in this paper is the single-layer cross-dipole structure, as shown in Fig. 1. The structure can achieve a phase shift range of approximately 330° while ensuring the independent regulation of dual-polarization. The cross-shaped metal branch is etched on the upper layer of the substrate, whose material is F4BM-2($\varepsilon_r = 2.2$). When changing the period of the element and the thickness of the substrate, different reflection characteristics can be obtained. Decreasing the element period can improve the linearity of the phase shift curve, but the phase-shift range will decrease. The thicker the dielectric substrate, the better the linearity of the phase-shift curve, but the phase shift range will be relatively reduced. Through the full-wave simulation optimization design, the structural parameters are chosen as follows: $D = 15$ mm, $H = 3$ mm, $W = 1$ mm. The simulation model is also shown in Fig. 1.

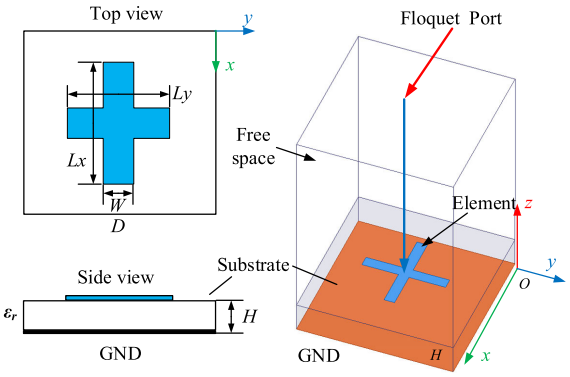

FIGURE 1. Model schematic of single-layer cross-dipole element.

Another important feature of the element is the ability to independently regulate dual-polarization incident waves. To analyze the performance, when the incident wave is with y-direction polarization, the element length in the fixed x-direction may be taken in three arbitrary values: $L_x = 3$, 8, 13 mm, the reflection phase characteristics versus element length in the y-direction with three phase shift curves are obtained and shown in Fig. 2(a). It can be seen that when changing the x-direction element length, the reflection phase in y-direction has hardly changed. Similarly, the situation of x-direction polarization can be observed in Fig. 2(b). The above is a good verification of the dual-polarization independent regulation characteristics of the cross-dipole element, so that different focus positions and focusing functions can be set according to the change of polarization of the incident waves, which further broadens the applications of the reflective metasurface.

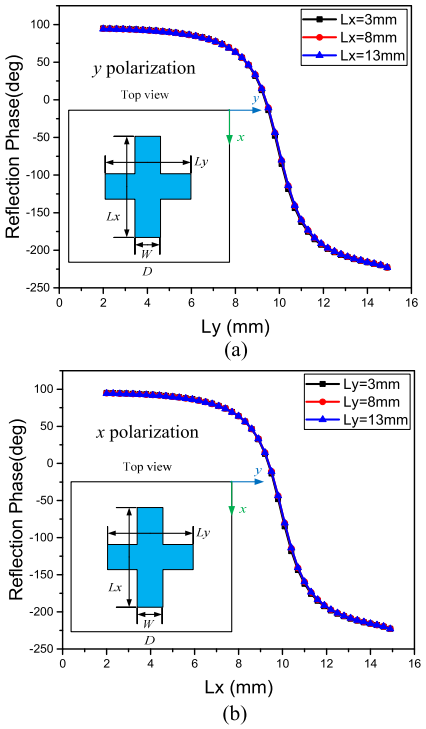

FIGURE 2. Reflection phase characteristics of polarization independent regulation: (a) Phase shift curve of *x*-direction element with *y*-direction polarization excitation; (b) Phase shift curve of *y*-direction element with *x*-direction polarization excitation.

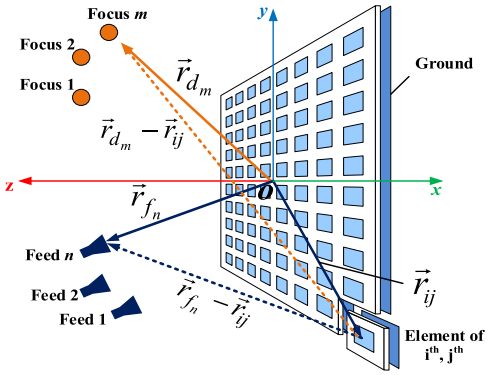

FIGURE 3. Model schematic of multi-feeds and multi-focus NFF reflective metasurface.

III. DESIGN OF NFF METASURFACE

A. MULTI-BEAM PHASE SYNTHESIS THEORY

The model schematic diagram of the NFF reflective metasurface shown in Fig. 3 is with the function of multi-feed power synthesis and multi-focus power distribution, which can realize the spatial diversity of wireless power. Based on the theory of multi-beams [26], it can be seen that the required E-field distribution of multi-focus can be obtained by superposing the E-field of each focus. Assume that m foci are to be generated at the locations $\vec{r}_{d_m}$, the superposition E-field of the metasurface is expressed as follows:

$$\begin{aligned} E_d(x_i, y_j) &= A_d(x_i, y_j) \cdot \exp(j\varphi_d(x_i, y_j)) \\ &= \sum_{m=1}^{M} A_m(x_i, y_j) \cdot \exp(j\varphi_m(x_i, y_j)) \end{aligned} \quad (1)$$

where (x_i, y_j) is the coordinate of the center of the metasurface element of the row i^{th} and column j^{th}. $A_m(x_i, y_j)$ is the amplitude of the required E-field, while $\varphi_m(x_i, y_j)$ is the phase. Since the amplitude excitation of each element of the reflected metasurface is determined by the feed excitation, when the conventional horn-fed is chosen, the amplitude excitation distribution $A_m(x_i, y_j)$ is determined. The distance between each element of the metasurface and the target focus is $\left|\vec{r}_{d_m} - \vec{r_{ij}}\right|$, and the expression of the phase distribution of m-focuses is

$$\varphi_d(x_i, y_j) = \arg\left\{\sum_{m=1}^{M}\left[D_m \exp(-jk_0\left|\vec{r}_{d_m} - \vec{r_{ij}}\right|)\right]\right\} \quad (2)$$

where D_m is the amplitude of E-field of the target focus, $k_0 = 2\pi/\lambda$ is the free-space wave number. It should be noted that by adjusting the ratio of D_m at different focuses, we can obtain unequal power distribution. This will also be discussed in detail in the latter part through simulation and measurement. When there are n feeds in the WPT system, in order to achieve maximum power transfer, it is necessary to correct the phase distribution of multiple feed excitations to the reflective metasurface, and the initial phase distribution $\varphi_f(x_i, y_j)$ is

$$\varphi_f(x_i, y_j) = \arg\left\{\sum_{n=1}^{N}\left[F_n \exp(jk_0\left|\vec{r}_{f_n} - \vec{r_{ij}}\right|)\right]\right\} \quad (3)$$

where F_n is the E-field amplitude of each feed. The total phase compensation can be achieved as follows:

$$\Delta\varphi_{ij}(x_i, y_j) = \varphi_d(x_i, y_j) - \varphi_f(x_i, y_j) \quad (4)$$

B. CASE1: SINGLE-FEED AND SINGLE-FOCUS WITH DUAL-POLARIZATION

To design a reflective metasurface with single-feed and single focus in dual-polarization, the location of the feed is $r_f = (0, 0, 0.2)$ m, which vertically illuminates the reflective metasurface at 10GHz. The focus of y- direction polarization is set at $r_d = (0.3, 0, 1)$ m, while of x-direction polarization is set at $r_d = (-0.3, 0, 1)$ m. The phase distribution on the reflective metasurface can be expressed in (5), which is also shown in Fig. 4.

$$\Delta\varphi_{ij}(x_i, y_j) = k_0(\left|\vec{r_f} - \vec{r_{ij}}\right| + \left|\vec{r_d} - \vec{r_{ij}}\right|) \quad (5)$$

The size of the 'cross-dipole' etched on each element is depending on the required reflection phase of the metasurface element, which is depicted in Fig. 4. According to the phase-size relationship extracted by element simulation in Section II, as shown in Fig. 2. The corresponding size topology of the designed metasurface could be obtained and observed in Fig. 5. With different colors, Fig. 5 shows the branch lengths distribution in the y and x directions of the cross-dipoles of the reflective metasurface. The designed reflective metasurface consists of 26 × 26 elements, whose top view of the simulation model is illustrated in Fig. 6. Each cross-dipole element of the metasurface is with the

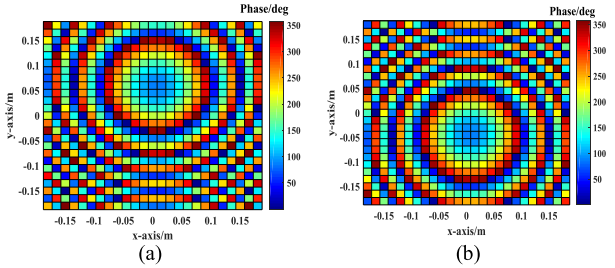

FIGURE 4. Phase distribution of single-feed and single-focus reflective metasurface: (a) *y*-direction polarization excitation; (b) *x*-direction polarization excitation.

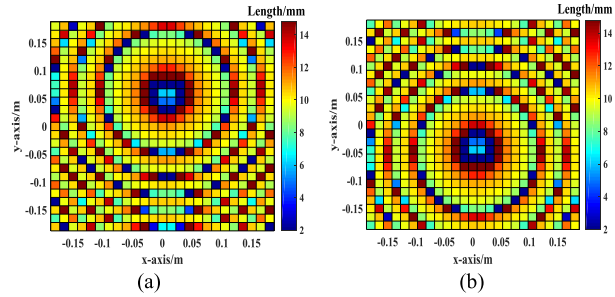

FIGURE 5. Size topology of single-feed and single-focus reflective metasurface: (a) *y*-direction polarization excitation; (b) *x*-direction polarization excitation.

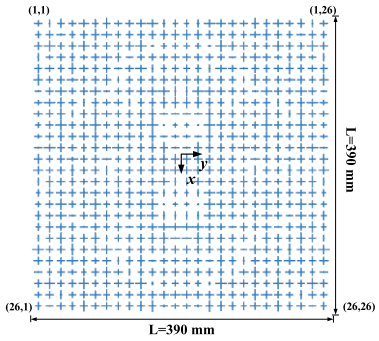

FIGURE 6. Geometry of single-feed and single-focus reflective metasurface in dual-polarization.

same width of 1 mm, and the lengths of y direction and x direction branches of the cross-dipoles are listed in TABLE 1 in detail. The overall size of the designed metasurface is 390 mm × 390 mm and the thickness is 3 mm. The material of the substrate is F4BM-2($\varepsilon_t = 2.2$).

Due to the dual-polarization independent regulation, the focus positions can be flexible arrangement for different polarization incident waves. It can be found from Fig. 7 that when the polarization direction of the incident wave changes, the position of the focus changes correspondingly, and the independent regulation of the dual polarization focus can be realized.

C. CASE2: SINGLE-FEED AND DUAL-FOCUS WITH DUAL-POLARIZATION FOR DIFFERENT POWER TRANSFER RATIO

This case is to design a new reflective metasurface for a single-feed and dual-focus with dual-polarization for

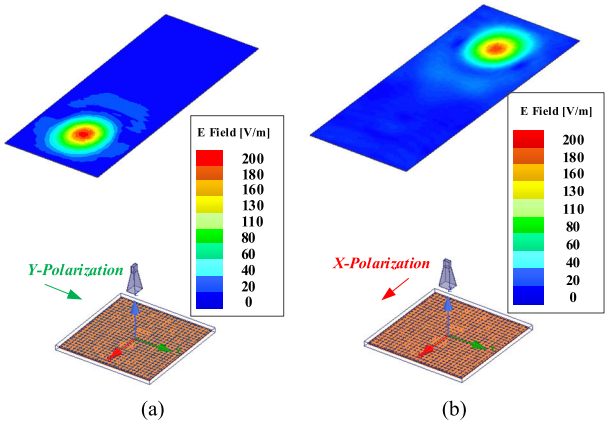

FIGURE 7. Full-wave simulation results of single-feed and single-focus metasurface: (a) *y*-direction polarization excitation; (b) *x*-direction polarization excitation.

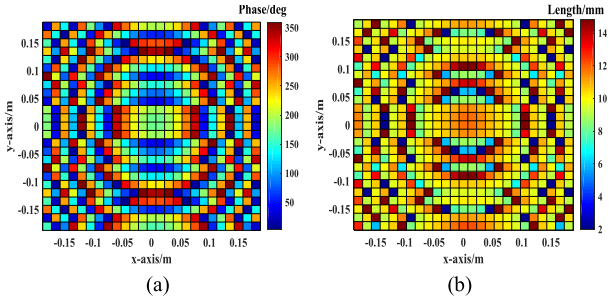

FIGURE 8. Single-feed and dual-focus metasurface in *y*-direction polarization excitation: (a) phase distribution; (b) size topology.

different power transfer system. The feed is set at $r_f = (0, 0, 0.2)$ m, vertically illuminates at 10 GHz. Two focuses in the situation of y direction polarization are respectively at $r_{d1} = (0.3, 0, 1)$ m, $r_{d2} = (-0.3, 0, 1)$ m, the ratio of the E-field amplitude of these two focuses is D_1: D_2 = 1:1. The required phase distribution is expressed in (6) and shown in Fig. 8(a). Fig. 8(b) shows the size topology in y-direction polarization of the desired metasurface. At the same time, for x-direction polarization, we change the amplitude ratio of D_1: D_2 to 1 : 1.2. The two focuses are set at $r_{d3} = (0, 0.3, 1)$ m and $r_{d4} = (0, -0.3, 1)$ m, respectively. The final designed geometry model is shown in Fig. 9, and the lengths of the cross-dipoles of the metasurface are listed in TABLE 2 in detail.

$$\Delta\varphi_{ij}(x_i, y_j) = k_0 \left|\vec{r_f} - \vec{r_{ij}}\right| - \arg\left\{\sum_{m=1}^{2}\left[D_m \exp(-jk_0 \left|\vec{r}_{d_m} - \vec{r_{ij}}\right|)\right]\right\} \quad (6)$$

The simulation results with y-direction polarization excitation are shown in Fig. 10(a). It can be seen that the two focuses are located at predetermined positions, and the E-field intensity distribution is almost uniform. It means that the equal power distribution of the designed metasurface is

TABLE 1. The dimension of the fabricated reflective metasurface in case 1 (unit: mm).

Elements		1	2	3	4	5	6	7	8	9	10	11	12	13	14	15	16	17	18	19	20	21	22	23	24	25	26
1	y	10.4	2	9.4	10.4	13.85	8.4	9.65	10.25	10.95	12.8	14.8	3.25	6.7	6.7	3.25	14.8	12.8	10.95	10.25	9.65	8.4	13.85	10.4	9.4	2	10.4
	x	7.7	9.95	11.6	8	9.75	10.6	14.1	7.55	9.25	9.75	10.05	10.25	10.4	10.4	10.25	10.05	9.75	9.25	7.55	14.1	10.6	9.75	8	11.6	9.95	7.7
2	y	7.75	9.95	11.6	8.05	9.75	10.6	14.35	7.7	9.3	9.8	10.1	10.3	10.45	10.45	10.3	10.1	9.8	9.3	7.7	14.35	10.6	9.75	8.05	11.6	9.95	7.75
	x	9.5	10.7	2.8	9.6	10.55	14.8	8.45	9.6	10.15	10.65	11.3	12.3	13.5	13.5	12.3	11.3	10.65	10.15	9.6	8.45	14.8	10.55	9.6	2.8	10.7	9.5
3	y	10.25	14.8	9.35	10.4	14.5	8.65	9.75	10.4	11.45	14.8	4.35	7.9	8.45	8.45	7.9	4.35	14.8	11.45	10.4	9.75	8.65	14.5	10.4	9.35	14.8	10.25
	x	10.1	13.65	9.15	10.25	12.85	8.3	9.7	10.35	11.25	14.8	2	7.6	8.25	8.25	7.6	2	14.8	11.25	10.35	9.7	8.3	12.85	10.25	9.15	13.65	10.1
4	y	2	9.7	11.05	6.8	9.65	10.55	13.9	7.75	9.35	9.85	10.15	10.4	10.55	10.55	10.4	10.15	9.85	9.35	7.75	13.9	10.55	9.65	6.8	11.05	9.7	2
	x	10.65	6.25	9.8	11.1	6.25	9.55	10.3	11.6	2	8.25	9.15	9.5	9.6	9.6	9.5	9.15	8.25	2	11.6	10.3	9.55	6.25	11.1	9.8	6.25	10.65
5	y	9.85	11.7	8.7	10.05	11.8	7.65	9.6	10.25	11.1	14.55	2	7.5	8.2	8.2	7.5	2	14.55	11.1	10.25	9.6	7.65	11.8	10.05	8.7	11.7	9.85
	x	11.8	8.95	10.25	14.8	9.05	10.1	11.2	2	8.7	9.5	9.9	10.1	10.2	10.2	10.1	9.9	9.5	8.7	2	11.2	10.1	9.05	14.8	10.25	8.95	11.8
6	y	11.85	8.95	10.3	14.8	9.1	10.1	11.35	2	8.85	9.6	9.95	10.15	10.3	10.3	10.15	9.95	9.6	8.85	2	11.35	10.1	9.1	14.8	10.3	8.95	11.85
	x	14.8	9.5	10.75	5.1	9.65	10.55	14.8	8.35	9.55	10	10.4	10.7	10.95	10.95	10.7	10.4	10	9.55	8.35	14.8	10.55	9.65	5.1	10.75	9.5	14.8
7	y	8.8	10.3	14.8	9.4	10.45	14.8	8.75	9.8	10.35	11.15	13.4	14.8	2	2	14.8	13.4	11.15	10.35	9.8	8.75	14.8	10.45	9.4	14.8	10.3	8.8
	x	2	9.8	11.5	8.4	9.95	11.2	2.3	9.25	9.95	10.45	11	11.85	12.75	12.75	11.85	11	10.45	9.95	9.25	2.3	11.2	9.95	8.4	11.5	9.8	2
8	y	10.1	14.8	9.4	10.55	2	9.35	10.2	11.35	2	8.35	9.25	9.6	9.7	9.7	9.6	9.25	8.35	2	11.35	10.2	9.35	2	10.55	9.4	14.8	10.1
	x	6.8	10	12.65	9	10.2	12.35	8	9.6	10.2	10.85	12.15	14.8	14.8	14.8	14.8	12.15	10.85	10.2	9.6	8	12.35	10.2	9	12.65	10	6.8
9	y	11.9	9.1	10.4	2	9.45	10.4	13.45	8.05	9.5	10	10.4	10.75	11	11	10.75	10.4	10	9.5	8.05	13.45	10.4	9.45	2	10.4	9.1	11.9
	x	7.55	10.05	13.95	9.2	10.3	14.05	8.6	9.75	10.4	11.3	14.55	2	2	2	2	14.55	11.3	10.4	9.75	8.6	14.05	10.3	9.2	13.95	10.05	7.55
10	y	7.6	10.05	14.3	9.25	10.35	14.65	8.75	9.8	10.45	11.5	14.8	2	5.75	5.75	2	14.8	11.5	10.45	9.8	8.75	14.65	10.35	9.25	14.3	10.05	7.6
	x	7.35	10.05	13.95	9.2	10.35	14.6	8.75	9.85	10.45	11.55	14.8	2	6.1	6.1	2	14.8	11.55	10.45	9.85	8.75	14.6	10.35	9.2	13.95	10.05	7.35
11	y	9.55	11.1	8.4	10.1	12.5	8.6	9.9	10.7	14.15	6.55	8.85	9.35	9.5	9.5	9.35	8.85	6.55	14.15	10.7	9.9	8.6	12.5	10.1	8.4	11.1	9.55
	x	5.2	9.95	12.55	9.05	10.25	13.25	8.5	9.75	10.4	11.35	14.8	2	4.85	4.85	2	14.8	11.35	10.4	9.75	8.5	13.25	10.25	9.05	12.55	9.95	5.2
12	y	10.2	14.8	9.65	10.95	6.85	9.7	10.6	14.8	8.1	9.35	9.8	10.1	10.2	10.2	10.1	9.8	9.35	8.1	14.8	10.6	9.7	6.85	10.95	9.65	14.8	10.2
	x	2	9.7	11.4	8.5	10.05	11.7	7.55	9.55	10.2	10.9	12.5	14.8	2	2	14.8	12.5	10.9	10.2	9.55	7.55	11.7	10.05	8.5	11.4	9.7	2
13	y	10.9	8.35	10.15	14.8	9.2	10.25	12.35	7.6	9.45	10	10.4	10.75	11.05	11.05	10.75	10.4	10	9.45	7.6	12.35	10.25	9.2	14.8	10.15	8.35	10.9
	x	12.8	9.35	10.7	5.7	9.75	10.85	2	9.15	9.9	10.45	11.1	12.2	13.7	13.7	12.2	11.1	10.45	9.9	9.15	2	10.85	9.75	5.7	10.7	9.35	12.8
14	y	12.8	9.35	10.7	5.7	9.75	10.85	2	9.15	9.9	10.45	11.1	12.2	13.7	13.7	12.2	11.1	10.45	9.9	9.15	2	10.85	9.75	5.7	10.7	9.35	12.8
	x	10.9	8.35	10.15	14.8	9.2	10.25	12.35	7.6	9.45	10	10.4	10.75	11.05	11.05	10.75	10.4	10	9.45	7.6	12.35	10.25	9.2	14.8	10.15	8.35	10.9
15	y	2	9.7	11.4	8.5	10.05	11.7	7.55	9.55	10.2	10.9	12.5	14.8	2	2	14.8	12.5	10.9	10.2	9.55	7.55	11.7	10.05	8.5	11.4	9.7	2
	x	10.2	14.8	9.6	10.95	6.85	9.7	10.6	14.8	8.1	9.35	9.8	10.1	10.2	10.2	10.1	9.8	9.35	8.1	14.8	10.6	9.7	6.85	10.95	9.6	14.8	10.2
16	y	5.15	9.95	12.55	9.05	10.25	13.25	8.55	9.75	10.4	11.35	14.8	2	4.85	4.85	2	14.8	11.35	10.4	9.75	8.55	13.25	10.25	9.05	12.55	9.95	5.15
	x	9.55	11.1	8.4	10.1	12.5	8.6	9.9	10.7	14.15	6.55	8.85	9.35	9.5	9.5	9.35	8.85	6.55	14.15	10.7	9.9	8.6	12.5	10.1	8.4	11.1	9.55
17	y	7.35	10.05	13.95	9.2	10.35	14.6	8.75	9.8	10.45	11.55	14.8	2	6.1	6.1	2	14.8	11.55	10.45	9.8	8.75	14.6	10.35	9.2	13.95	10.05	7.35
	x	7.65	10.1	14.3	9.25	10.35	14.65	8.75	9.8	10.45	11.5	14.8	2	5.8	5.8	2	14.8	11.5	10.45	9.8	8.75	14.65	10.35	9.25	14.3	10.1	7.65
18	y	7.55	10.05	14	9.2	10.3	14.05	8.65	9.75	10.4	11.3	14.5	2	2	2	2	14.5	11.3	10.4	9.75	8.65	14.05	10.3	9.2	14	10.05	7.55
	x	11.9	9.1	10.4	2	9.45	10.4	13.5	8.05	9.5	10	10.4	10.75	11	11	10.75	10.4	10	9.5	8.05	13.5	10.4	9.45	2	10.4	9.1	11.9
19	y	6.8	10	12.65	9	10.2	12.35	8	9.6	10.2	10.85	12.15	14.8	14.8	14.8	14.8	12.15	10.85	10.2	9.6	8	12.35	10.2	9	12.65	10	6.8
	x	10.1	14.8	9.4	10.55	2	9.35	10.2	11.35	2	8.35	9.25	9.6	9.7	9.7	9.6	9.25	8.35	2	11.35	10.2	9.35	2	10.55	9.4	14.8	10.1
20	y	2	9.8	11.5	8.4	9.95	11.2	2.3	9.25	9.95	10.45	11	11.85	12.75	12.75	11.85	11	10.45	9.95	9.25	2.3	11.2	9.95	8.4	11.5	9.8	2
	x	8.75	10.3	14.8	9.4	10.45	14.8	8.75	9.8	10.35	11.15	13.4	14.8	2	2	14.8	13.4	11.15	10.35	9.8	8.75	14.8	10.45	9.4	14.8	10.3	8.75
21	y	14.8	9.5	10.75	5.1	9.65	10.55	14.8	8.35	9.55	10	10.4	10.7	10.95	10.95	10.7	10.4	10	9.55	8.35	14.8	10.55	9.65	5.1	10.75	9.5	14.8
	x	11.85	8.95	10.3	14.8	9.1	10.1	11.35	2	8.85	9.6	9.95	10.2	10.3	10.3	10.2	9.95	9.6	8.85	2	11.35	10.1	9.1	14.8	10.3	8.95	11.85
22	y	11.8	8.95	10.25	14.8	9.05	10.1	11.2	2	8.7	9.5	9.85	10.1	10.2	10.2	10.1	9.85	9.5	8.7	2	11.2	10.1	9.05	14.8	10.25	8.95	11.8
	x	9.85	11.7	8.7	10.1	11.8	7.65	9.6	10.25	11.1	14.55	2	7.5	8.2	8.2	7.5	2	14.55	11.1	10.25	9.6	7.65	11.8	10.1	8.7	11.7	9.85
23	y	10.65	6.25	9.8	11.1	6.25	9.55	10.3	11.6	2	8.25	9.15	9.5	9.6	9.6	9.5	9.15	8.25	2	11.6	10.3	9.55	6.25	11.1	9.8	6.25	10.65
	x	2	9.7	11.05	6.8	9.65	10.55	13.9	7.75	9.35	9.85	10.15	10.4	10.55	10.55	10.4	10.15	9.85	9.35	7.75	13.9	10.55	9.65	6.8	11.05	9.7	2
24	y	10.05	13.65	9.1	10.25	12.85	8.3	9.7	10.35	11.25	14.8	2	7.6	8.25	8.25	7.6	2	14.8	11.25	10.35	9.7	8.3	12.85	10.25	9.1	13.65	10.05
	x	10.25	14.8	9.35	10.4	14.5	8.65	9.75	10.4	11.45	14.8	4.35	7.9	8.45	8.45	7.9	4.35	14.8	11.45	10.4	9.75	8.65	14.5	10.4	9.35	14.8	10.25
25	y	9.5	10.7	2.8	9.6	10.55	14.8	8.45	9.6	10.15	10.65	11.3	12.3	13.5	13.5	12.3	11.3	10.65	10.15	9.6	8.45	14.8	10.55	9.6	2.8	10.7	9.5
	x	7.75	9.95	11.6	8.05	9.75	10.6	14.35	7.7	9.3	9.8	10.1	10.3	10.45	10.45	10.3	10.1	9.8	9.3	7.7	14.35	10.6	9.75	8.05	11.6	9.95	7.75
26	y	7.75	9.95	11.6	8	9.75	10.6	14.1	7.55	9.25	9.75	10.05	10.25	10.4	10.4	10.25	10.05	9.75	9.25	7.55	14.1	10.6	9.75	8	11.6	9.95	7.75
	x	10.4	2	9.4	10.4	13.85	8.4	9.65	10.25	10.95	12.8	14.8	3.25	6.7	6.7	3.25	14.8	12.8	10.95	10.25	9.65	8.4	13.85	10.4	9.4	2	10.4

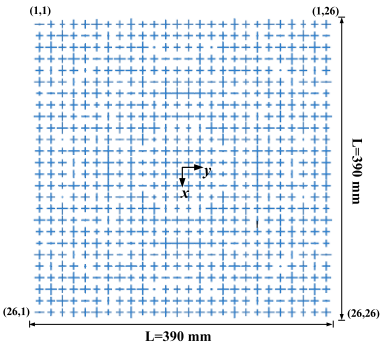

FIGURE 9. Geometry of single-feed, dual-focus reflective metasurface with dual-polarization for different power transfer ratio.

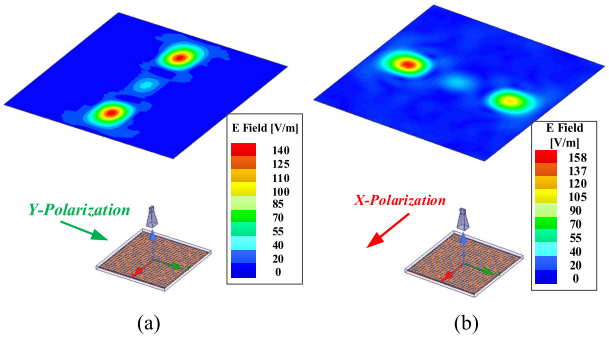

FIGURE 10. Full-wave simulation results of single-feed dual-focus metasurface: (a) *y*-direction polarization excitation; (b) *x*-direction polarization excitation.

well realized. Then let the feed horn rotate 90° around z axis, which means the horn is rotated on the azimuth plane and the incident angle is unchanged. Thus the incident wave is changed as x-direction polarization, and the simulation results are shown in Fig. 10(b). The two preset focus positions are unchanged, and the E-field intensity distribution has obvious strength change, which realizes the unequal power distribution of dual-focus. The next step, let the feed horn rotate 45° around z axis, which can excite the dual-polarization incident waves simultaneously. The simulation results show that the four focuses are achieved by using multi-focus design and independent regulation of dual polarization, as shown in Fig. 11. However, it is worth pointing out that since the horn feed is not an ideal point source, so it is difficult

TABLE 2. The dimension of the fabricated reflective metasurface in case 2 (unit: mm).

Elements		1	2	3	4	5	6	7	8	9	10	11	12	13	14	15	16	17	18	19	20	21	22	23	24	25	26
1	y	12.65	9	5.8	9.65	10.55	14.6	8.25	9.5	10.05	10.5	11	11.6	12.15	12.15	11.6	11	10.5	10.05	9.5	8.25	14.6	10.55	9.65	5.8	9	12.65
	x	3.5	9.05	10.15	11.8	10.6	13.45	7.5	9	2	7.5	8.7	11.75	11.55	11.4	10.8	8.95	7.5	14.8	9.7	7.85	13	10.3	13	10.2	8.9	10.7
2	y	8.95	10.3	14.8	9.1	10.15	11.45	2	9.05	9.75	10.15	10.55	10.85	11.1	11.1	10.85	10.55	10.15	9.75	9.05	2	11.45	10.15	9.1	14.8	10.3	8.95
	x	9.85	10.3	14.8	8.9	5.7	9.3	10	10.45	9.7	10.05	10.35	9.1	9	8.95	8.05	10.45	10.05	9.6	11.3	10.05	9.25	14.8	9.2	14.8	10.25	2
3	y	10.15	14.8	9.25	10.3	13.55	8.5	9.75	10.35	11.35	14.8	2.15	7.75	8.35	8.35	7.75	2.15	14.8	11.35	10.35	9.75	8.5	13.55	10.3	9.25	14.8	10.15
	x	11.65	14.8	9.25	10.2	9.8	10.55	12.85	2	11.25	14.1	2	10.5	10.4	10.35	10.1	2	14.15	11	8.5	13.5	10.5	9.5	10.35	9.25	14.7	9.4
4	y	12.25	9.05	10.3	14.8	9	10	11	14.8	8.25	9.35	9.75	9.95	10.05	10.05	9.95	9.75	9.35	8.25	14.8	11	10	9	14.8	10.3	9.05	12.25
	x	8.5	9.2	10.3	13.8	11.15	2	9	9.65	8.25	9.25	9.6	2	2	2	13.55	9.7	9.25	7.65	10.05	9.1	2	10.6	14.8	10.3	9.05	10.25
5	y	10.45	2	9.65	10.85	2	9.45	10.2	11.3	14.8	7.95	9.05	9.45	9.55	9.55	9.45	9.05	7.95	14.8	11.3	10.2	9.45	2	10.85	9.65	2	10.45
	x	9.95	10.15	13.5	8.85	6.75	9.45	10.15	10.75	9.95	10.35	10.75	9.55	9.5	9.45	9.05	10.95	10.35	9.85	12	10.2	9.35	2	9.1	13.65	10.1	11.9
6	y	13.2	9.3	10.5	2	9.4	10.3	12.3	6.85	9.25	9.8	10.15	10.4	10.55	10.55	10.4	10.15	9.8	9.25	6.85	12.3	10.3	9.4	2	10.5	9.3	13.2
	x	11.1	11.6	8.45	9.95	9.6	10.35	12.05	2	11.25	14.65	2	10.6	10.55	10.45	10.15	4.25	14.65	11	8.2	12.4	10.3	9.2	10.1	8.5	11.3	6.15
7	y	7.7	10.05	13.15	9.05	10.2	12.2	7.8	9.55	10.15	10.75	11.7	13.95	14.8	14.8	13.95	11.7	10.75	10.15	9.55	7.8	12.2	10.2	9.05	13.15	10.05	7.7
	x	2	4.3	9.75	10.9	10.4	12.45	7.65	9.3	4.8	8.75	9.35	14.8	14.8	14.8	11.8	9.5	8.75	2	9.75	7.95	12.15	10.05	11.15	9.75	2	9.3
8	y	9.4	10.8	7.15	9.85	11.2	6.5	9.55	10.25	11.2	14.8	5.75	8.25	8.7	8.7	8.25	5.75	14.8	11.2	10.25	9.55	6.5	11.2	9.85	7.15	10.8	9.4
	x	8.95	9.15	10.35	14.8	12	7.1	9.5	10.05	9.35	9.8	10.15	8.8	8.7	8.55	6.55	10.25	9.8	9.15	10.45	9.55	6.55	10.9	2	10.35	9	9.9
9	y	14.8	9.65	11.1	7.95	9.9	11.1	2	9.25	9.95	10.5	11.15	12.2	13.6	13.6	12.2	11.15	10.5	9.95	9.25	2	11.1	9.9	7.95	11.1	9.65	14.8
	x	9.7	9.8	11.3	7.95	2	9.3	10.1	10.8	10	10.45	11	9.75	9.7	9.65	9.3	11.25	10.45	9.9	11.9	10.15	9.2	14.8	8.5	11.35	9.7	10.4
10	y	7.5	10.05	14.1	9.25	10.35	14.65	8.75	9.8	10.45	11.5	14.8	2	5.95	5.95	2	14.8	11.5	10.45	9.8	8.75	14.65	10.35	9.25	14.1	10.05	7.5
	x	10.1	10.2	14.8	9.25	8.65	9.85	10.7	13	10.55	11.5	14.7	10.25	10.2	10.2	9.9	14.8	11.5	10.4	2	10.75	9.8	6.15	9.4	14.8	10.1	11.05
11	y	8.85	10.4	2	9.65	10.85	2	9.4	10.2	11.1	14.8	5.8	8.35	8.75	8.75	8.35	5.8	14.8	11.1	10.2	9.4	2	10.85	9.65	2	10.4	8.85
	x	10.45	10.6	2	9.65	9.35	10.15	11.6	2	11.3	14.8	3.55	10.8	10.7	10.65	10.3	6.8	14.8	11	7.9	11.75	10.15	8.65	9.8	2.55	10.45	12.15
12	y	11.15	8.7	10.25	14.8	9.35	10.35	13.35	8.15	9.55	10.05	10.5	10.95	11.25	11.25	10.95	10.5	10.05	9.55	8.15	13.35	10.35	9.35	14.8	10.25	8.7	11.15
	x	10.8	10.95	7.75	9.9	9.65	10.45	13.6	7.05	12.7	2	8.1	11.45	11.3	11.2	10.6	8.55	2	11.9	8.85	14.3	10.4	9.2	10	7.8	10.8	14.65
13	y	11.5	9	10.4	2	9.5	10.5	14.8	8.65	9.7	10.2	10.7	11.25	11.75	11.75	11.25	10.7	10.2	9.7	8.65	14.8	10.5	9.5	2	10.4	9	11.5
	x	11	11.2	8.35	10	9.75	10.6	14.8	8.05	14.6	6	8.6	12.05	11.85	11.65	10.85	8.9	5.95	12.85	9.1	14.8	10.55	9.35	10.1	8.35	11	14.8
14	y	11.5	9	10.4	2	9.5	10.5	14.8	8.65	9.7	10.2	10.7	11.25	11.75	11.75	11.25	10.7	10.2	9.7	8.65	14.8	10.5	9.5	2	10.4	9	11.5
	x	11	11.2	8.35	10	9.75	10.6	14.8	8.05	14.6	6	8.6	12.05	11.85	11.65	10.85	8.9	5.95	12.85	9.1	14.8	10.55	9.35	10.1	8.35	11	14.8
15	y	11.15	8.7	10.25	14.8	9.35	10.35	13.35	8.15	9.55	10.05	10.5	10.95	11.25	11.25	10.95	10.5	10.05	9.55	8.15	13.35	10.35	9.35	14.8	10.25	8.7	11.15
	x	10.8	10.95	7.75	9.9	9.65	10.45	13.6	7.05	12.7	2	8.1	11.45	11.3	11.2	10.6	8.55	2	11.9	8.85	14.3	10.4	9.2	10	7.8	10.8	14.65
16	y	8.85	10.4	2	9.65	10.85	2	9.4	10.2	11.1	14.8	5.8	8.35	8.75	8.75	8.35	5.8	14.8	11.1	10.2	9.4	2	10.85	9.65	2	10.4	8.85
	x	10.45	10.6	2	9.65	9.35	10.15	11.6	2	11.3	14.8	3.55	10.8	10.7	10.65	10.3	6.8	14.8	11	7.9	11.75	10.15	8.65	9.8	2.55	10.45	12.15
17	y	7.5	10.05	14.1	9.25	10.35	14.65	8.75	9.8	10.45	11.5	14.8	2	5.95	5.95	2	14.8	11.5	10.45	9.8	8.75	14.65	10.35	9.25	14.1	10.05	7.5
	x	10.1	10.2	14.8	9.25	8.65	9.85	10.7	13	10.55	11.5	14.7	10.25	10.2	10.2	9.9	14.8	11.5	10.4	2	10.75	9.8	6.15	9.4	14.8	10.1	11.05
18	y	14.8	9.65	11.1	7.95	9.9	11.1	2	9.25	9.95	10.5	11.15	12.2	13.6	13.6	12.2	11.15	10.5	9.95	9.25	2	11.1	9.9	7.95	11.1	9.65	14.8
	x	9.7	9.8	11.3	7.95	2	9.3	10.1	10.8	10	10.45	11	9.75	9.7	9.65	9.3	11.25	10.45	9.9	11.9	10.15	9.2	14.8	8.5	11.35	9.7	10.4
19	y	9.4	10.8	7.15	9.85	11.2	6.5	9.55	10.25	11.2	14.8	5.75	8.25	8.7	8.7	8.25	5.75	14.8	11.2	10.25	9.55	6.5	11.2	9.85	7.15	10.8	9.4
	x	8.95	9.15	10.35	14.8	12	7.1	9.5	10.05	9.35	9.8	10.15	8.8	8.7	8.55	6.55	10.25	9.8	9.15	10.45	9.55	6.55	10.9	2	10.35	9	9.9
20	y	7.7	10.05	13.15	9.05	10.2	12.2	7.8	9.55	10.15	10.75	11.7	13.95	14.8	14.8	13.95	11.7	10.75	10.15	9.55	7.8	12.2	10.2	9.05	13.15	10.05	7.7
	x	2	4.3	9.75	10.9	10.4	12.45	7.65	9.3	4.8	8.75	9.35	14.8	14.8	14.8	11.8	9.5	8.75	2	9.75	7.95	12.15	10.05	11.15	9.75	2	9.3
21	y	13.2	9.3	10.5	2	9.4	10.3	12.3	6.85	9.25	9.8	10.15	10.4	10.55	10.55	10.4	10.15	9.8	9.25	6.85	12.3	10.3	9.4	2	10.5	9.3	13.2
	x	11.1	11.6	8.45	9.95	9.6	10.35	12.05	2	11.25	14.65	2	10.6	10.55	10.45	10.15	4.25	14.65	11	8.2	12.4	10.3	9.2	10.1	8.5	11.3	6.15
22	y	10.45	2	9.65	10.85	2	9.45	10.2	11.3	14.8	7.95	9.05	9.45	9.55	9.55	9.45	9.05	7.95	14.8	11.3	10.2	9.45	2	10.85	9.65	2	10.45
	x	9.95	10.15	13.5	8.85	6.75	9.45	10.15	10.75	9.95	10.35	10.75	9.55	9.5	9.45	9.05	10.95	10.35	9.85	12	10.2	9.35	2	9.1	13.65	10.1	11.9
23	y	12.25	9.05	10.3	14.8	9	10	11	14.8	8.25	9.35	9.75	9.95	10.05	10.05	9.95	9.75	9.35	8.25	14.8	11	10	9	14.8	10.3	9.05	12.25
	x	8.5	9.2	10.3	13.8	11.15	2	9	9.65	8.25	9.25	9.6	2	2	2	13.55	9.7	9.25	7.65	10.05	9.1	2	10.6	14.8	10.3	9.05	10.25
24	y	10.15	14.8	9.25	10.3	13.55	8.5	9.75	10.35	11.35	14.8	2.15	7.75	8.35	8.35	7.75	2.15	14.8	11.35	10.35	9.75	8.5	13.55	10.3	9.25	14.8	10.15
	x	11.65	14.8	9.25	10.2	9.8	10.55	12.85	2	11.25	14.1	2	10.5	10.4	10.35	10.1	2	14.15	11	8.5	13.5	10.5	9.5	10.35	9.25	14.7	9.4
25	y	8.95	10.3	14.8	9.1	10.15	11.45	2	9.05	9.75	10.15	10.55	10.85	11.1	11.1	10.85	10.55	10.15	9.75	9.05	2	11.45	10.15	9.1	14.8	10.3	8.95
	x	9.85	10.3	14.8	8.9	5.7	9.3	10	10.45	9.7	10.05	10.35	9.1	9	8.95	8.05	10.45	10.05	9.6	11.3	10.05	9.25	14.8	9.2	14.8	10.25	2
26	y	12.65	9	5.8	9.65	10.55	14.6	8.25	9.5	10.05	10.5	11	11.6	12.15	12.15	11.6	11	10.5	10.05	9.5	8.25	14.6	10.55	9.65	5.8	9	12.65
	x	3.5	9.05	10.15	11.8	10.6	13.45	7.5	9	2	7.5	8.7	11.75	11.55	11.4	10.8	8.95	7.5	14.8	9.7	7.85	13	10.3	13	10.2	8.9	10.7

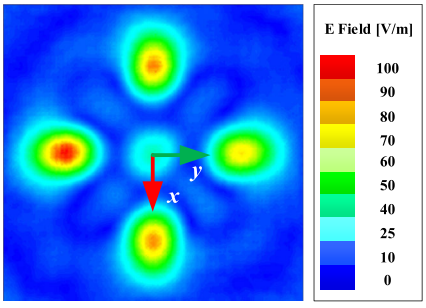

FIGURE 11. Full-wave simulation results of *E*-field intensity distribution of single-feed and dual-focus metasurface in dual-polarization.

to achieve ideal equality of two polarization components by rotating the horn 45°, and the focal E-field intensity distribution is with certain differences.

IV. MEASUREMENTS OF NFF METASURFACE

A. NEAR-FIELD SCANNING MEASUREMENT

According to the full-wave simulation in the previous section, the reflective metasurface with the same size and parameters are actually fabricated. The broadband horn working at 2-18 GHz is set as a feeding source and placed at $r_f = (0, 0, 0.2)$ m for vertical illumination. The experimental system is shown in Fig. 12(a). The measurement was carried out in a microwave anechoic chamber, and the designed NFF reflective metasurface was measured by planar near-field scanning. The scanning range is 1 m $\times$ 0.4 m, the distance between the 10 GHz standard probe and the metasurface is 1m. This is consistent with the size of the designed metasurface in the full-wave simulation. The measurement system is shown in Fig. 12(b). For the case of single-feed and single-focus (corresponding to Section III Part B), the reflective metasurface with the same parameters shown in Fig. 6 is fabricated and measured. The dimension of each cross-dipole element of the metasurface are listed in Table 1 in detail. Through rotating the horn around z axis to obtain different polarization excitations, we obtain the measurement results, as shown in Fig. 13. Figs. 13(a) and (b) are the y-direction polarization and x-direction polarization, respectively. Comparing with Fig. 7, it can be seen that the measured and simulated results are in good agreement, which further verifies the effectiveness of the NFF design.

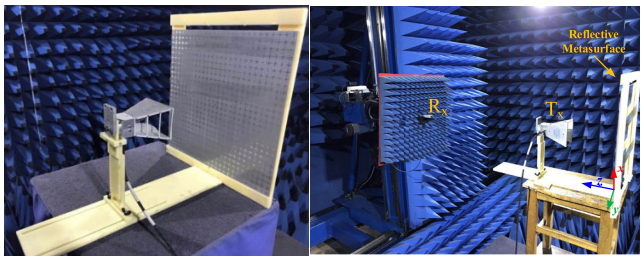

(a) (b)

FIGURE 12. Measurement system of the designed reflective metasurface, (a) prototype of single-feed and single-focus dual-polarization metasurface, (b) near-field scanning measurement system.

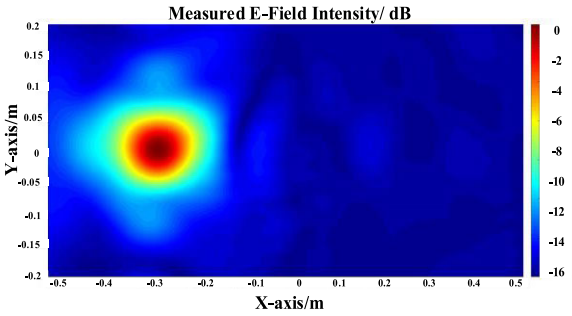

(a)

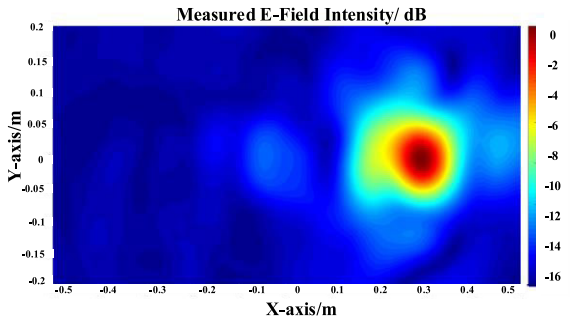

(b)

FIGURE 13. The normalized measurement results of reflective *E*-field intensity distribution: (a) *y*-direction polarization excitation; (b) *x*-direction polarization excitation.

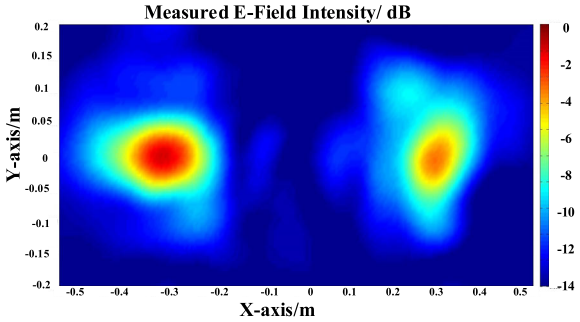

FIGURE 14. The normalized measurement results of reflective *E*-field intensity for single-feed and single-focus reflective metasurface in 40° polarization excitation.

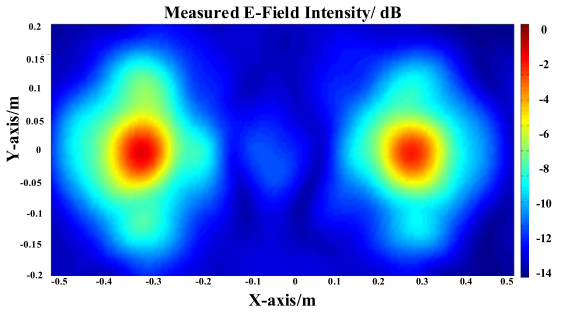

(a)

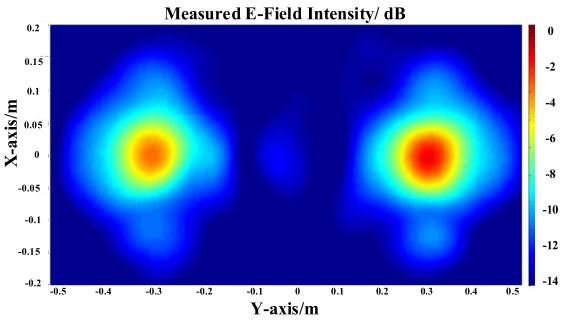

(b)

FIGURE 15. The normalized measurement results of reflective *E*-field intensity for single-feed and dual-focus metasurface: (a) equal power distribution in *y*-direction polarization excitation; (b) unequal power distribution in *x*-direction polarization excitation.

The dual-focus focusing system can also be achieved by changing the angle around z axis of the feed horn. If the feed horn is rotated by 40° on the azimuth plane and the incident angle unchanged, it will be decomposed into two waves with different intensities but orthogonal polarization directions incident to the metasurface. Keeping other parameters unchanged and rotating the horn 40°, we can get the measurement results, as shown in Fig.14. It can be found that the two focuses are produced and located at the preset positions of $r_{dx} = (-0.3, 0, 1)$ m in x-polarization and $r_{dy} = (0.3, 0, 1)$ m in y-polarization, respectively. Since the horn is not an ideal point source and the block effect of the support structure, the focus is not completely symmetrical in the actual measurement. However, the position of the maximum E-field intensity is consistent with the design, which verifies the effectiveness of the reflective metasurface to realize NFF.

For the case of single-feed and dual-focus (corresponding to Section III Part C), a reflective metasurface with the same parameters shown in Fig. 9 is fabricated and measured, whose dimension in detail is mentioned in Table 2. Fig. 15(a) shows the measured E-field distribution with equal-power transfer in the y-direction polarization excitation, while Fig. 15(b) shows the measured E-field distribution with the unequal-power transfer in the x-direction polarization excitation. Comparing with Fig. 10, the measured and simulated results are in good agreement.

B. 10 GHZ NFF-WPT SYSTEM MEASUREMENT

This NFF-WPT system measurement is used to verify the superiority of NFF. The transmission system is shown in Fig. 12, and all the equipment and parameters are kept the same as the near-field scanning measurement of case 1, i.e., the single-feed and single-focus WPT system.

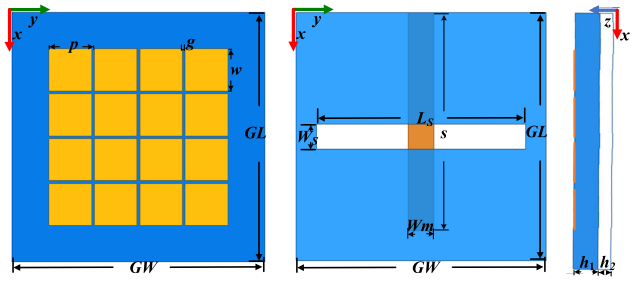

FIGURE 16. The geometry of the proposed slot-coupling metasurface antenna working at 10 GHz as the receiver of the WPT system measurement: (a) top view of the 4×4 mushroom metasurface; (b) top view of the microstrip-line aperture structure; (c) side view.

A slot-coupling metasurface antenna is designed and fabricated to play the role of the receiver, as shown in Fig. 16. It is composed of a three-layers structure: a 4 × 4 mushroom metasurface structure is the top layer, the slot-coupling ground is the second layer, and the bottom layer is a metal microstrip feedline. The thickness of the upper layer substrate is $h_1 = 1.5$ mm, while the lower is $h_2 = 0.8$ mm. Both the two substrates are made of F4B material with permittivity of 2.65. The size of the proposed metasurface antenna is 18 mm × 18 mm × 2.3 mm.The geometry of the designed antenna is shown in Fig. 16 and the optimized dimensions are shown in Table 3. The detailed design process can be seen in [27]–[29]. The simulated and measured S_{11} and the prototype of the designed receiving antenna are shown in Fig. 17.

TABLE 3. Dimensions of the designed metasurface antenna (unit: mm).

p	g	w	GL	GW	h_1
3.2	0.2	3	18	18	1.5
Ls	Ws	Wm	s	h_2	
15	1.82	1.85	15.8	0.8	

In order to detect the receiving power, we connect the receiving antenna with a power senor (RS-NRP18S) as a load. The position of the receiving antenna is set at the preset focus position, i.e. $r_d = (0.3, 0, 1)$ m. The power received by the metasurface antenna can be detected by the power sensor. It is worth mentioning that the receiver is smaller than 2 cm in size, thus it can be completely situated within the core region of the focusing aperture with the highest power density, which is helpful to verify the actual performance of NFF transmission.

As a reference for comparing NFF transfer performance, we define the non-NFF transfer as follows. Keeping the transmitting power and working frequency consistent with the NFF transfer, the same feed horn points directly at the receiving antenna position, where the preset focus is in NFF transfer case. Since the transmission distance and the receiving antenna are identical, the focusing transfer performance of NFF can be verified by comparing the wireless power obtained by the receiving antenna. The measured results are shown in Table 4, and it can be found that the receiving power using NFF is 15 dB higher than that using non-NFF transmission at the same distance. After several tests with or without the power amplifier (+25 dB), a stable verification result can be obtained. Therefore, combined with the previous near-field scanning measurement, the superiority and high-efficiency of NFF transfer system realized by reflective metasurface for WPT is verified.

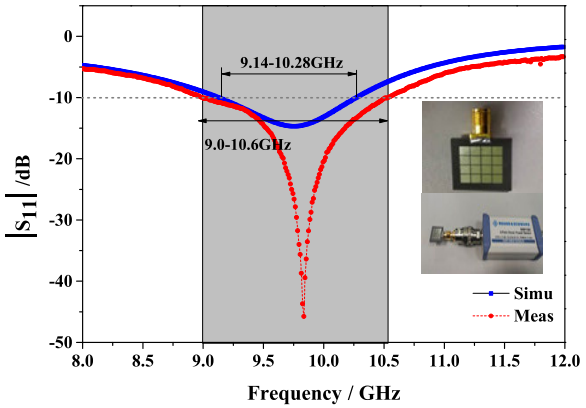

FIGURE 17. Measured and simulated reflection coefficient, the prototype of the proposed metasurface antenna, and the proposed antenna connected with a RS-NRP18S power sensor.

TABLE 4. The receiving power by the metasurface antenna of NFF transfer and NON-NFF transfer.

	NFF	Non-NFF
P_{in}=-2 dBm	-18~-20 dBm	-35 dBm
P_{in}=-2 dBm+PA（25 dB）	5 dBm	-10 dBm

V. ANALYSIS OF NFF REFLECTIVE METASURFACE CHARACTERISTICS

A. COMPARISION BETWEEN NFF REFLECTIVE METASURFACE AND TRADITIONAL DIRECTIONAL-BEAM REFLECTARRAY

The NFF reflective metasurface proposed in this paper is different from the traditional directional-beam reflectarray. The NFF is designed for focusing in the near-field region (including Fresnel region), while the traditional directional-beam reflectarray is designed for radiation in far-field region. In order to further analyze the characteristic difference between the former and the latter, the far-field radiation patterns of two cases are simulated respectively. As shown in Fig. 18, the NFF reflective metasurface in the far field has

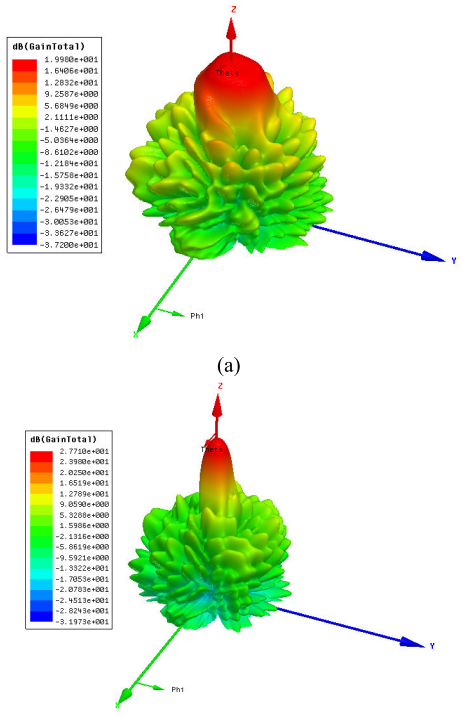

FIGURE 18. The far-field radiation characteristics: (a) NFF reflective metasurface; (b) traditional directional-beam reflectarray.

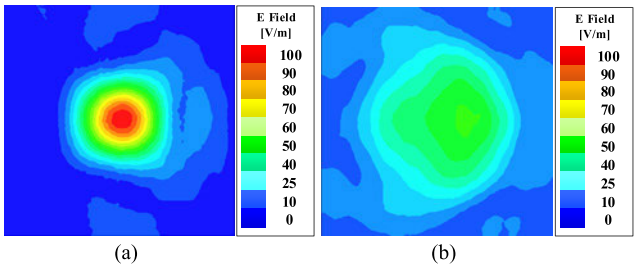

FIGURE 19. *E*-field intensity distribution of the reference plane in the near-field: (a) NFF reflective metasurface; (b) traditional directional-beam reflectarray.

the wider main beam and the beam pointing is in the same direction as the focus position. In the far-field, the directional-beam reflectarray has the narrower main beam and E-field intensity distribution is more concentrated.

Then, the characteristics of beam-concentrating of two cases are analyzed and compared in the near-field region, as shown in Fig. 19. The focus of the NFF metasurface is set at $r_d = (0, 0, 1)$ m, while the main beam direction is set along the vector $(\theta_r, \varphi_r) = (0^\circ, 0^\circ)$. And thus we set the observational plane as the 1 meter away from them. In this case, the distance of 1 m is within the near-field region. Through full-wave simulation, the E-field intensity distribution of the reference plane can be observed in Fig. 19. Obviously it can be found that the E-field intensity distribution of the NFF reflective metasurface is more prominent for power convergence. The area of the focusing aperture of the NFF reflective

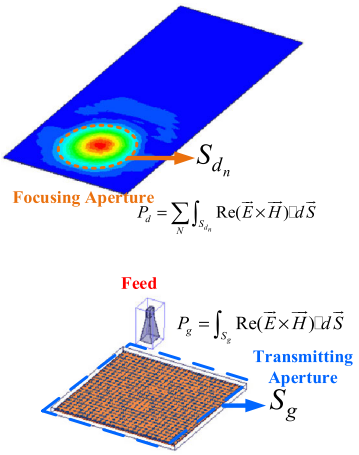

FIGURE 20. Schematic diagram of NFF transfer efficiency calculation.

metasurface is smaller than that of the traditional directional-beam reflectarray. This also illustrates the characteristics of NFF transfer, and the beam is concentrated in the near-field region, and then relatively diverge to the far-field region.

B. NFF TRANSFER EFFICIENCY ANALYSIS

This part is mainly to discuss the transfer efficiency of the NFF reflective metasurface. NFF transfer efficiency η can be determined by the ratio of P_d (the power of the focus aperture captures on the reference plane) and P_g (the power of the metasurface aperture captures from the feed). As shown in Fig. 20, S_d and S_g are respectively the area of the focusing aperture on the observational plane in the near-field region and the physical aperture of NFF reflective metasurface. P_d and P_g can be calculated by using numerical integration based on Poynting theorem. Wireless power transmitted from the feed illuminates on the reflective metasurface. The Poynting vector integration is performed on the aperture of the metasurface, and the power captured by the metasurface aperture, the P_g, can be calculated according to the formula shown in Fig. 20. After the regulation and reflection of the metasurface, the wireless power in the form of focused beam illuminates on the focusing aperture, and P_d could be obtained by the Poynting vector integration on the focusing aperture, in the same manner.

By means of full-wave simulation, the NFF transfer efficiency curve is obtained and shown in Fig. 21. The four curves shown in Fig. 21 are respectively: 1) MTS indicates the power capture efficiency of the metasurface, which is defined as the ratio of the power of the NFF metasurface aperture captures power from the horn; 2) 1T1R1P indicates the NFF transfer efficiency of the case that single-feed and single-focus in single polarization excitation; 3)1T2R1P indicates the NFF transfer efficiency of the case that single-feed and dual-focus in single polarization excitation; 4)1T1R2P indicates the NFF transfer efficiency of the case that single-feed and single-focus in dual polarization excitation. Wherein for 3) and 4), the entire NFF transfer efficiency is the sum of the efficiency of each focus.

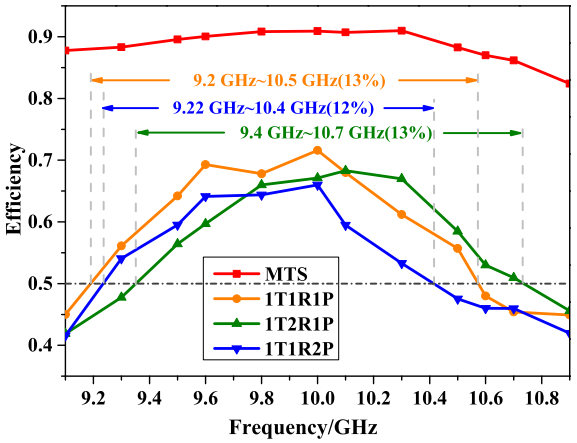

FIGURE 21. Full-wave simulation results of NFF transfer efficiency varying with frequency: MTS: the power capture efficiency of the metasurface; 1T1R1P: the NFF transfer efficiency of single-feed and single-focus in single polarization excitation; 1T2R1P: the NFF transfer efficiency of single-feed and dual-focus in single polarization excitation; 1T1R2P: the NFF transfer efficiency of single-feed and single-focus in dual polarization excitation.

It can be found from Fig. 21 that the case of 1T1R1P is with the maximum efficiency at the operating frequency 10 GHz, 71.6%. The relative bandwidth with 50% NFF transfer efficiency is 13%, from 9.2 GHz to 10.5 GHz. The curves of 1T2R1P and 1T1R2P are with the similar trends. Compared with the case of single-focus, the maximum efficiency of these two cases has a small range of decline. It is because the decomposition of the polarization component and the design of the multi-beam will introduce a certain beam dispersion, so that the total power on the focusing aperture decreases. For the case of 1T2R1P, the relative bandwidth is 13%, from 9.4 GHz to 10.7 GHz, and the maximum efficiency is 68.3%; while for the case of 1T1R2P, the relative bandwidth is about 12%, from 9.2 GHz to 10.4 GHz, and the maximum efficiency is 65.9%. For the WPT system, the performance of the relative bandwidth with 50% NFF transfer efficiency of all the cases above are guaranteed.

C. NFF TRANSFER PERFORMANCE ANALYSIS

In theory, within the near-field region of the transmitting antenna (range $R \leq 2D^2/\lambda$), high efficient NFF transfer is available. But in fact, microwave is difficult to maintain the propagation characteristics as ideal light wave. No matter what kind of antenna, such as microstrip phased arrays, or reflective metarsurface, can not completely converge electromagnetic waves to some certain ideal points in space. The resulting phenomenon deserves attention: a) When the transmitting antenna aperture remains the same and the NFF transfer distance increases, although the focus is still in the near-field region, the focusing ability of the beam is declining. In other words, NFF cannot guarantee the efficient power transfer of the same transmitting aperture in the whole near-field region. b) The E-field intensity at the center of focusing aperture is generally not the point with the maximum E-field intensity in the radial direction of the transmission path, which is also be demonstrated in [5], [22].

Set the feed horn at $r_f = (0, 0, 0.2)$ m and give the y-direction polarization excitation, and set the focus with different focusing distance. The preset focus are respectively at $r_{d1} = (0.3, 0, 0.5)$ m, $r_{d2} = (0.3, 0, 1)$ m, $r_{d3} = (0.3, 0, 2)$ m and $r_{d4} = (0.3, 0, 5)$ m, which means that the focusing distance in the radial direction is respectively 0.5 m, 1 m, 2 m, 5 m. A single-feed, single-focus NFF reflective metasurface with the size of 390 mm × 390 mm(13λ × 13λ) working at 10GHz is designed.

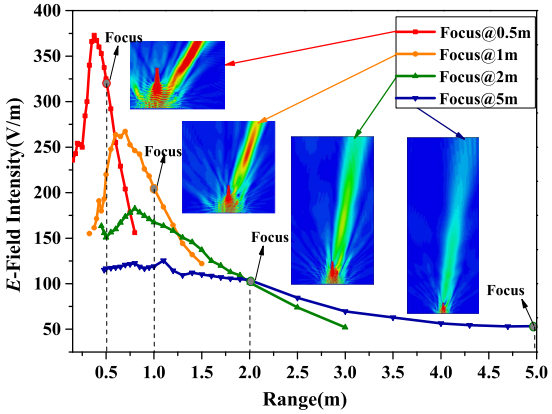

FIGURE 22. The full-wave simulation results of the E-field intensity distribution of different preset focusing distance and the curves of the E-field intensity varying with distance in the radial direction.

The full-wave simulation results of the E-field intensity distribution of the above four cases and the curves of the E-field intensity varying with distance in the radial direction are shown in Fig. 22. When the focus is set at 0.5m in the radial direction, the maximum E-field intensity occured at 0.4 m, and for the cases of 1 m, 2 m and 5 m, the maximum E-field intensity occurred respectively at 0.7 m, 0.8 m and 1.1 m. It can be found that in the case that the preset focusing distance is set as 5 m (167λ), the focusing beam may diverge before reaching the preset focusing aperture. This indicates that there is a constraint relationship between the NFF performance and the electrical size of the transmitting aperture.The longer the preset focusing distance is, the larger the difference between the E-field intensity at the center of the focusing aperture and the maximum E-field intensity in the radial direction, the weaker the convergence ability of the beam. When the preset focusing distance is too long, even if the focus is still within the near-field region, the beam will also diverge, making it difficult to realize ideal NFF transfer.

Fig. 23 gives the E-field intensity distribution of the focusing plane when the preset focus of the reflective metasurface is respectively at $r_{d1} = (0.3, 0, 0.5)$ m, $r_{d2} = (0.3, 0, 1)$ m and $r_{d3} = (0.3, 0, 2)$ m. It is not hard to find that, the closer the focus is to the reflective metasurface, the narrower focus beam is gotten, the smaller size of focusing aperture is gotten, and the larger E-field intensity at the center of the focusing aperture is also gotten.

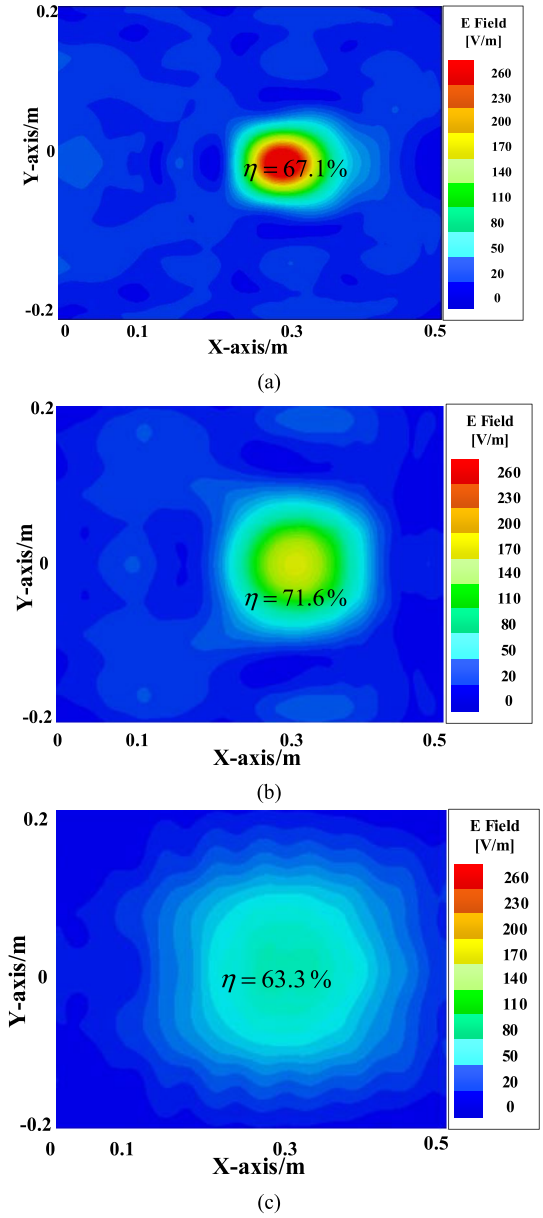

FIGURE 23. *E*-field intensity distribution of the focusing plane for cases that the focus is set at: (a) $r_{d1} = (0.3, 0, 0.5)$ m; (b) $r_{d2} = (0.3, 0, 1)$ m; (c) $r_{d3} = (0.3, 0, 2)$ m.

However, it is worth noting that the concentrated distribution of *E*-field intensity on the focusing plane is not equivalent to the high NFF transfer efficiency of the main beam on the focusing plane. Integrating the Poynting vector on the focusing aperture and calculating the NFF transfer efficiency for the above cases, the results of 0.5 m, 1 m and 2 m are respectively 67.1%, 71.6% and 63.3%. The case of 1m(33.3λ) has the maximum NFF transfer efficiency, and the beam is also relatively concentrated. When the focus is set at 0.5 m(16.7λ), it is too close to the reflective metasurface. It will result in a strong coupling field above the aperture of the reflective metasurface, and form strong side lobes in other directions, thus reducing the NFF transfer efficiency. It does not mean that the closer the preset focus distance is away from the reflective metasurface, the higher the NFF transfer efficiency of the focusing beam will be.

VI. CONCLUSION

This paper presents a new design of NFF reflective metasurface which can realize multi-focus and high-efficiency power transfer. Thanks to the dual-polarization independent regulation and the synthetical phase regulation of the designed metasurface, multi-focus beams with independent unequal power distribution can be realized in the near-field region.The single-feed, single-focus and single-feed, dual-focus metasurfaces working at 10 GHz are farbricated and measured by planar near-field scanning. To form a WPT system, A slot-coupling metasurface antenna is also designed as the power receiver. The experiment results show that for the same receiver and the same transfer condition, the receiving power of the NFF transfer realized by the proposed reflective metasurface is 15 dB higher than non-NFF transfer. The maximum NFF focusing efficiency can reach 71.6%. It verifies the effectiveness of the NFF reflective metasurface for WPT system. Through further analysis, it is found that NFF beam has higher beam convergence performance than the traditional high-gain beam in the near-field region. Choosing the appropriate ratio between the electrical size of the reflective metasurface and the focusing distance can ensure the optimal focusing performance.

REFERENCES

[1] J. Garnica, R. A. Chinga, and J. Lin, "Wireless power transmission: From far field to near field," *Proc. IEEE*, vol. 101, no. 6, pp. 1321–1331, Jun. 2013.

[2] T. Arakawa, S. Goguri, J. V. Krogmeier, A. Kruger, D. J. Love, R. Mudumbai, and M. A. Swabey, "Optimizing wireless power transfer from multiple transmit coils," *IEEE Access*, vol. 6, pp. 23828–23838, 2018.

[3] A. Kurs, A. Karalis, R. Moffatt, J. D. Joannopoulos, P. Fisher, and M. Soljačić, "Wireless power transfer via strongly coupled magnetic resonances," *Science*, vol. 317, no. 5834, pp. 83–86, 2007.

[4] W. C. Brown, "The history of power transmission by radio waves," *IEEE Trans. Microw. Theory Techn.*, vol. MTT-32, no. 9, pp. 1230–1242, Sep. 1984.

[5] F. Musavi and W. Eberle, "Overview of wireless power transfer technologies for electric vehicle battery charging," *IET Power Electron.*, vol. 7, no. 1, pp. 60–66, Jan. 2014.

[6] J. Sherman, "Properties of focused apertures in the Fresnel region," *IRE Trans. Antennas Propag.*, vol. 10, no. 4, pp. 399–408, Jul. 1962.

[7] R. C. Hansen, "Focal region characteristics of focused array antennas," *IEEE Trans. Antennas Propag.*, vol. AP-33, no. 12, pp. 1328–1337, Dec. 1985.

[8] L. Shafai, A. A. Kishk, and A. Sebak, "Near field focusing of apertures and reflector antennas," in *Proc. WESCANEX, Commun., Power Comput. Conf.*, May 1997, pp. 246–251.

[9] J. Bor, S. Clauzier, O. Lafond, and M. Himdi, "60 GHz foam-based antenna for near-field focusing," *Electron. Lett.*, vol. 50, no. 8, pp. 571–572, Apr. 2015.

[10] A. Buffi, P. Nepa, and G. Manara, "Design criteria for near-field-focused planar arrays," *IEEE Antennas Propag. Mag.*, vol. 54, no. 1, pp. 40–50, Feb. 2012.

[11] F. Tofigh, J. Nourinia, M. Azarmanesh, and K. M. Khazaei, "Near-field focused array microstrip planar antenna for medical applications," *IEEE Antennas Wireless Propag. Lett.*, vol. 13, pp. 951–954, 2014.

[12] R. Siragusa, P. Lemaitre-Auger, and S. Tedjini, "Tunable near-field focused circular phase-array antenna for 5.8-GHz RFID applications," *IEEE Antennas Wireless Propag. Lett.*, vol. 10, pp. 33–36, 2011.

[13] K. D. Stephan, J. B. Mead, D. M. Pozar, L. Wang, and J. A. Pearce, "A near field focused microstrip array for a radiometric temperature sensor," *IEEE Trans. Antennas Propag.*, vol. 55, no. 4, pp. 1199–1203, Apr. 2007.
[14] S. Karimkashi and A. A. Kishk, "Focusing properties of Fresnel zone plate lens antennas in the near-field region," *IEEE Trans. Antennas Propag.*, vol. 59, no. 5, pp. 1481–1487, May 2011.
[15] I. V. Minin and O. V. Minin, *Basic Principles of Fresnel Antenna Arrays* (Lecture Notes in Electrical Engineering), vol. 19. Berlin, Germany: Springer-Verlag, 2008.
[16] A. J. Martinez-Ros, J. L. Gómez-Tornero, F. J. Clemente-Fernández, and J. Monzó-Cabrera, "Microwave near-field focusing properties of width-tapered microstrip leaky-wave antenna," *IEEE Trans. Antennas Propag.*, vol. 61, no. 6, pp. 2981–2990, Jun. 2013.
[17] J. L. Gómez-Tornero, D. Blanco, E. Rajo-Iglesias, and N. Llombart, "Holographic surface leaky-wave lenses with circularly-polarized focused near-fields—Part I: Concept, design and analysis theory," *IEEE Trans. Antennas Propag.*, vol. 61, no. 7, pp. 3475–3485, Jul. 2013.
[18] P. Lemaitre-Auger, R. Siragusa, C. Caloz, and D. Kaddour, "Circular antenna arrays for near-field focused or multi-focused beams," in *Proc. Int. Symp. Electromagn. Theory*, May 2013, pp. 425–428.
[19] Y. J. Cheng and F. Xue, "Ka-band near-field-focused array antenna with variable focal point," *IEEE Trans. Antennas Propag.*, vol. 64, no. 5, pp. 1725–1732, May 2016.
[20] O. Yurduseven, D. L. Marks, J. N. Gollub, and D. R. Smith, "Design and analysis of a reconfigurable holographic metasurface aperture for dynamic focusing in the Fresnel zone," *IEEE Access*, vol. 5, pp. 15055–15065, 2017.
[21] P.-F. Li, S.-W. Qu, S. Yang, Y. Liu, and Q. Xue, "Near-field focused array antenna with frequency-tunable focal distance," *IEEE Trans. Antennas Propag.*, vol. 66, no. 7, pp. 3401–3410, Jul. 2018.
[22] N. Yu, P. Genevet, M. A. Kats, F. Aieta1, J.-P. Tetienne, F. Capasso, and Z. Gaburro1, "Light propagation with phase discontinuities: Generalized laws of reflection and refraction," *Science*, vol. 334, no. 6054, pp. 333–337, Oct. 2011.
[23] A. M. Shaltout, A. V. Kildishev, and V. M. Shalaev, "Evolution of photonic metasurfaces: From static to dynamic," *J. Opt. Soc. Amer. B, Opt. Phys.*, vol. 33, no. 3, pp. 501–510, 2016.
[24] Y. Yuan, K. Zhang, X. Ding, B. Ratni, S. N. Burokur, and Q. Wu, "Complementary transmissive ultra-thin meta-deflectors for broadband polarization-independent refractions in the microwave region," *Photon. Res.*, vol. 7, no. 1, pp. 80–88, Jan. 1, 2019.
[25] Z. Wang, X. Ding, K. Zhang, B. Ratni, S. N. Burokur, X. Gu, and Q. Wu, "Huygens metasurface holograms with the modulation of focal energy distribution," *Adv. Opt. Mater.*, vol. 6, no. 12, Jun. 2018, Art. no. 1800121.
[26] X. Ding, F. Monticone, K. Zhang, L. Zhang, D. Gao, S. N. Burokur, A. de Lustrac, Q. Wu, C.-W. Qiu, and A. Alù, "Ultrathin Pancharatnam–Berry metasurface with maximal cross-polarization efficiency," *Adv. Mater.*, vol. 27, no. 7, pp. 1195–1200, Feb. 2015.
[27] H.-T. Chou, T.-M. Hung, N.-N. Wang, H.-H. Chou, C. Tung, and P. Nepa, "Design of a near-field focused reflectarray antenna for 2.4 GHz RFID reader applications," *IEEE Trans. Antennas Propag.*, vol. 59, no. 3, pp. 1013–1018, Mar. 2011.
[28] X. Wu, X. Xia, J. Tian, Z. Liu, and W. Wen, "Broadband reflective metasurface for focusing underwater ultrasonic waves with linearly tunable focal length," *Appl. Phys. Lett.*, vol. 108, no. 16, p. 163502(1-5), 2016.
[29] S. Zhang, M. H. Kim, F. Aieta, A. She, T. Mansuripur, I. Gabay, M. Khorasaninejad, D. Rousso, X. Wang, and M. Troccoli, "High efficiency near diffraction-limited mid-infrared flat lenses based on metasurface reflectarrays," in *Lasers Electro-Optics*, pp. 18024–18034, 2016.
[30] S. Yu, H. Liu, and L. Li, "Design of near-field focused metasurface for high-efficient wireless power transfer with multifocus characteristics," *IEEE Trans. Ind. Electron.*, vol. 66, no. 5, pp. 3993–4002, May 2019.
[31] P. Nayeri, F. Yang, and A. Z. Elsherbeni, "Design and experiment of a single-feed quad-beam reflectarray antenna," *IEEE Trans. Antennas Propag.*, vol. 60, no. 2, pp. 1166–1171, Feb. 2012.
[32] W. Liu, Z. N. Chen, and X. Qing, "Metamaterial-based low-profile broadband mushroom antenna," *IEEE Trans. Antennas Propag.*, vol. 62, no. 3, pp. 1165–1172, Mar. 2014.
[33] Z. Wu, L. Li, X. Chen, and K. Li, "Dual-band antenna integrating with rectangular mushroom-like superstrate for WLAN applications," *IEEE Antennas Wireless Propag. Lett.*, vol. 15, pp. 1269–1272, 2016.

PEI ZHANG was born in Yangzhou, China, in 1992. He received the B.E. degree in radio wave propagation and antenna from Xidian University, Xi'an, China, in 2017, where he is currently pursuing the Ph.D. degree in electromagnetic fields and microwave technology.

His research interests include wireless power transfer, wireless energy harvesting, metasurfaces, and electromagnetic field simulation and optimization.

LONG LI (M'06–SM'11) was born in Guizhou, China. He received the B.E. and Ph.D. degrees in electromagnetic fields and microwave technology from Xidian University, Xi'an, China, in 1998 and 2005, respectively, where he joined the School of Electronic Engineering, in 2005, and became a Full Professor, in 2010.

He was a Senior Research Associate with the Wireless Communications Research Center, City University of Hong Kong, in 2006. He received the Japan Society for Promotion of Science (JSPS) Postdoctoral Fellowship and visited Tohoku University, Sendai, Japan, as a JSPS Fellow, from November 2006 to November 2008. He was a Senior Visiting Scholar with Pennsylvania State University, USA, from December 2013 to July 2014. He is currently a Full Professor with the School of Electronic Engineering, Xidian University. He is the Director of the Key Laboratory of High Speed Circuit Design and EMC, Ministry of Education, China. He has authored or coauthored over 100 papers in refereed journal. His research interests include metamaterials, computational electromagnetics, electromagnetic compatibility, novel antennas, and wireless power transfer and harvesting technology.

Prof. Li is a Senior Member of the Chinese Institute of Electronics (CIE). He received the Nomination Award of National Excellent Doctoral Dissertation of China, in 2007. He won the Best Paper Award in the International Symposium on Antennas and Propagation, in 2008. He received the Program for New Century Excellent Talents in University of the Ministry of Education of China, in 2010. He received the First Prize of Awards for Scientific Research Results offered by Shaanxi Provincial Department of Education, China, in 2013. He received the IEEE APS Raj Mittra Travel Grant Senior Researcher Award, in 2014. He received the Shaanxi Youth Science and Technology Award, in 2016.

XUANMING ZHANG was born in Xi'an, China, in 1992. He is currently pursuing the Ph.D. degree in electromagnetic fields and microwave technology with Xidian University, Xi'an. His research interests include metasurfaces design, wireless power transfer, and wireless energy harvesting.

He received the National Scholarship for doctoral students, in 2017, the First Prize of the Key Laboratory of High Speed Circuit Design and EMC of Ministry of Education Academic Annual Conference, in 2017, Xidian University, and the Honorable Mention in Mathematical Contest in Modeling (MCM), in 2013.

HAIXIA LIU (M'13) was born in Hebei, China, in 1976. She received the B.S. and M.S. degrees in test and measurement technique and instrumentation and the Ph.D. degree in electromagnetic fields and microwave technology from Xidian University, Xi'an, China, in 1998, 2001, and 2014, respectively.

In 2001, she studied at Shizuoka University, Shizuoka, Japan, as a Cooperative Graduate. Since 2002, she has been with Xidian University. Her research interests include circuit analysis, frequency measurement and control, wireless power transfer, antennas, and electromagnetic compatibility.

YAN SHI (M'07–SM'16) received the B.Eng. and Ph.D. degrees in electromagnetic fields and microwave technology from Xidian University, Xi'an, China, in 2001 and 2005, respectively, where he joined the School of Electronic Engineering, in 2005, and became a Full Professor, in 2011.

From 2007 to 2008, he was a Senior Research Associate with the City University of Hong Kong, Hong Kong. From 2009 to 2010, he was a Visiting Postdoctoral Research Associate with the University of Illinois at Urbana-Champaign, Champaign, IL, USA. He has authored or coauthored over 100 papers in refereed journal and one book entitled Notes on Catastrophe Theory (Sci. Press, 2015). His current research interests include computational electromagnetics, metamaterial, antenna, and electromagnetic compatibility. He is a Senior Member of the Chinese Institute of Electronics. He received the Program for New Century Excellent Talents in University awarded by the Ministry of Education of China, in 2011, the New Scientific and Technological Star of Shaanxi Province awarded by the Education Department of Shaanxi Provincial Government, in 2013, the First Prize for the Scientific Research Results of High Education of Shaanxi Province awarded by the Education Department of the Shaanxi Provincial Government, in 2013, and the Second Prize of Awards of Science and Technology awarded by the Shaanxi Province Government, in 2015.